Theoretical analysis of screened heat pipes for medium and high temperature solar applications

2014 J. Phys.: Conf. Ser. 547 012010

(http://iopscience.iop.org/1742-6596/547/1/012010)

Journal of Physics: Conference Series **547** (2014) 012010 doi:10.1088/1742-6596/547/1/012010

Theoretical analysis of screened heat pipes for medium and high temperature solar applications

P Di Marco, S Filippeschi, A Franco, D Jafari*

Università di Pisa, DESTEC, Largo Lucio Lazzarino 2, 56122 Pisa, Italy

E-mail: d.jafari@studenti.unipi.it

Abstract. A mathematical model is applied to study the cylindrical heat pipes (HPs) behaviour when it is exposed to higher heat input at the evaporator for solar collector applications. The steady state analytical model includes two-dimensional heat conduction in the wall, the liquid flow in the wick and vapour hydrodynamics, and can be used to evaluate the working limits and to optimize the HP. The results of the analytical model are compared with numerical and experimental results available in literature, with good agreement. The effects of heat transfer coefficient, power input, evaporator length, pipe diameter, wick thickness and effective pore radius on the vapour temperature, maximum pressure drop and maximum heat transfer capability (HTC) of the HP are studied. The analysis shows that wick thickness plays an important role in the enhancement of HTC. Results show that it is possible to improve HTC of a HP by selecting the appropriate wick thickness, effective pore radius, and evaporator length. The parametric investigations are aimed to determine working limits and thermal performance of HP for medium temperature solar collector application.

1. Introduction

The HP is a two-phase device that transfers heat from a hot zone to a cold zone using capillary forces generated by a wick and a working fluid. The thermal performance of a HP can be characterized by its overall thermal resistance and its maximum power. These characteristics depend mainly on the capillary structure, which is usually made of grooves, meshes, sintered powder or a combination of them.

The interest in the use of HPs is recognized in many industrial applications such as control of satellites and spacecraft in aerospace, the cooling of electronic components and solar applications. Interesting connection can be evidenced in the literature between solar collector and HPs. The HPs that can be applied are based both on the conventional scheme in which the capillary action permits to return heat to the evaporator or according to the scheme of the wickless HP or closed loop two-phase thermosyphon working in gravity mode [1,2] or antigravity mode [3]. Recently, there has been a rising interest in the use of HP technology in the solar collector. Chun et al. [4] experimentally studied a particular system using different working fluids. Joudi and Witwit [5] used various lengths copper pipe with water as a working fluid. Mathioulakis and Belessiotis [6] presented the energy behaviour of a solar collector employing a HP filled with ethanol. Riffat et al. [7] investigated thermal performance of a thin membrane of HP solar collector. Azad [8] developed a theoretical model for analysing HP parameters. Taoufik et al. [9] developed the thermal efficiency of a flat plate HP solar collector. Finally, Aghbalou et al. [10] used HP in parabolic solar collector.

As a result of the interest in HP technology, several analytical and numerical analyses have been developed by many investigators. There has been a considerable research in the area of HP modelling from simple state thermodynamic analyses [11] and transient one dimensional (1-D) [12] to multidimensional [13-17].
As a result of the interest in HP technology, several analytical and numerical analyses have been developed by many investigators. Analytical modelling has been extensively carried on by researchers, with particular concern for fundamental analyses related to hydrodynamic and heat transfer processes [18-20]. Several models have been developed to predict the pressure drop that occurs in HPs; researchers used the Darcy's law [15, 16, 20] and non-Darcian transport [14, 21]. Evaporation and condensation at liquid–vapour interface have been described using the conjugate heat transfer model [14], and liquid–vapour coupling by means of interfacial velocity [16, 20]. In the case of thermal resistances of the wall and wick, researchers neglected conduction in the wall [18, 19, 21], considered heat conduction in radial direction [14], or in the axial direction [16], or the two-dimensional [20].
The specific objective of this paper is to investigate the HP for solar collectors, considering in particular the temperature range between 60 and 160°C, temperature range of specific interest for solar cooling and industrial process heat. The mathematical model presented in this paper is based on Shabgard and Faghri's model [16] and constituted a useful tool to perform optimization and parametric studies as well as to evaluate the HP capillary limits. The two dimensional steady state analytical model implemented in a MATLAB platform that couples axisymmetric heat conduction in the wall to liquid flow in the wick and vapour flow in the core. The results of the present model were compared to a numerical and experimental results reported in [13], and to an analytical model [14]. A very good agreement was observed.
Although several studies reveal the large potential of HP for solar collector, little attention has been paid to study the HP behaviour when it is exposed to high heat inputs at the evaporator. This paper presents a parametric study of the effect of different operation parameters on the HP performance. The effects of the wick thickness, the outside diameter (OD), the evaporator length, the power input, and the cooling fluid heat transfer coefficient of the condenser are studied. The motivation was to determine what are the effects on the heat transport behaviour of the screen wick structure, whether an optimum wick structure exists and how the value for maximum heat removal for a wick structure is determined for medium to high temperature solar application.

2. Mathematical model

The HP model is shown in figure 1a: it consists of the wall, the porous wick, and the vapour space in the radial direction as well as three sections in the axial direction (evaporator, adiabatic and condenser). As schematically shown in the thermal network, two-dimensional heat conduction in the wall is coupled with the 1-D heat conduction in the wick (radial). According to the electrical analogy (figure 1b), the radial and the axial heat conduction can be modelled as thermal resistances.

$$R_{radial} = \frac{\ln r_2 / r_1}{2\pi k L} \tag{1}$$

$$R_{axial} = \frac{L}{kA} \tag{2}$$

Where r_1 and r_2 are the radial locations of the inner and outer surfaces of the element, respectively, k is the conductivity of the material, A is the cross section, $A = \pi(r_2^2 - r_1^2)$ and L is the length of the given zone. In case of solid wall k is the thermal conductivity of the pure material; concerning the wick, the effective conductivity (k_{eff}) takes into account the thermal conductivity of both liquid and metal.

$$k_{eff} = \frac{k_l\left[(k_l + k_w) - (1-\varepsilon)(k_l - k_w)\right]}{\left[(k_l + k_w) + (1-\varepsilon)(k_l - k_w)\right]} \tag{3}$$

where k_l and k_w are the thermal conductivities liquid and wick material, respectively and ε is the wick porosity. As schematically evidenced in figure 1b, there are two possible pathways for the conductive heat transfer through the HP, from the evaporator to the condenser. The thermal resistance of path 1 and 2, neglecting radial thermal resistance of the wall, can be described as

$$\text{Path 1: } R_{W,e} + R_{W,c} \tag{4}$$

$$\text{Path 2: } R_{3P,e} + R_{1P,a} + \frac{R_{2P,a}(R_{1W,a} + R_{2W,a})}{R_{2P,a} + R_{1W,a} + R_{2W,a}} + R_{3P,a} + R_{3P,c} \tag{5}$$

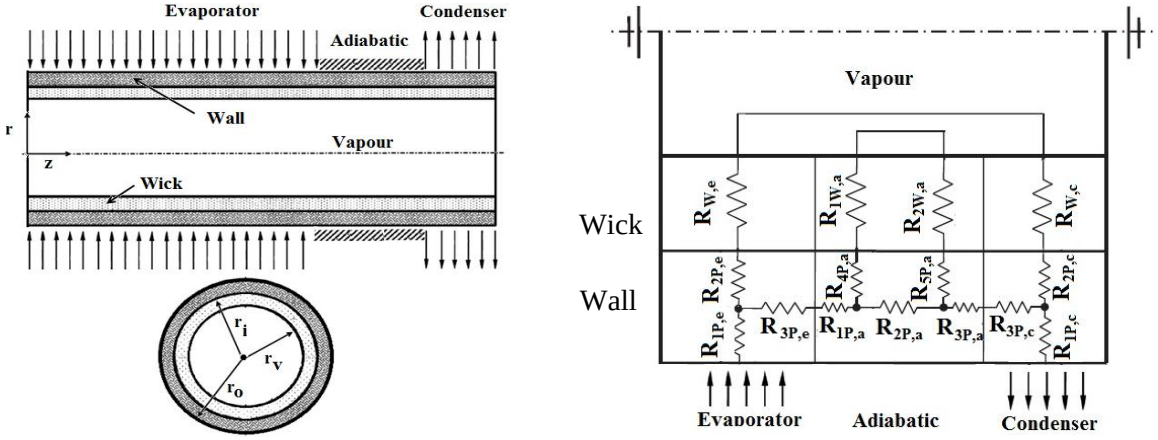

(a) (b)

Figure 1. (a) Schematic view of the cylindrical HP. (b) Network scheme for solid model (P, Pipe(wall); W, wick; e, evaporator; a, adiabatic; c, condenser)

The assumptions in the analysis are steady-state, incompressible and laminar flow, a saturated wick, constant properties and saturation temperature, and linear temperature profile across the thin wick structure. The conservation of mass, momentum, and energy equation is defined as follows.

- Heat conduction in the wall

The energy equation for two-dimensional (figure 1) and steady-state heat conduction in the wall with constant properties can be written as (θ is difference between the wall temperature and vapour temperature)

$$\frac{\partial^2\theta}{\partial r^2} + \frac{1}{r}\frac{\partial\theta}{\partial r} + \frac{\partial^2\theta}{\partial z^2} = 0 \tag{6}$$

- Liquid flow in wick

Continuity equation and Darcy's law [22] is used for the liquid flow in the porous wick:

$$r\frac{\partial u_l}{\partial z} + \frac{\partial}{\partial r}(rv_l) = 0 \tag{7}$$

$$u_l = -\frac{K}{\mu_l}\frac{dP_l}{dz} \tag{8}$$

where u_l is axial and v_l is radial liquid velocity, K is medium permeability, μ_l is liquid dynamic viscosity, and P_l is liquid pressure.

- Vapour flow analysis

A parabolic velocity profile is used for vapour flow within the HP. The conservation equations for mass and momentum are used to obtain vapour velocity and pressure in the core:

$$r\frac{\partial u_v}{\partial z}+\frac{\partial}{\partial r}(rv_v)=0 \tag{9}$$

$$\rho_v\left(u_v\frac{\partial u_v}{\partial z}+v_v\frac{\partial u_v}{\partial r}\right)=-\frac{\partial P_v}{\partial z}+\mu_v\left(\frac{\partial u_v}{\partial r^2}+\frac{1}{r}\frac{\partial u_r}{\partial r}\right) \tag{10}$$

where ρ_v is density, u_v is axial velocity, v_v is radial velocity, P_v is pressure, and μ_v is vapour dynamic viscosity.

- Liquid-vapour interface

At the interface the vapour velocity is related to the liquid velocity by a mass balance:

$$\rho_v v_{v,i}=\rho_l v_{l,i} \tag{11}$$

Boundary condition specifications at the outer pipe (r_o), wall-wick (r_i), wick-vapour interface (r_v) as well as at center axis and both ends of HP, are provided in table 1. A MATLAB platform is used to discretize the governing equations. In order to validate the model, the analytical results are compared with the experimental data reported in literature [13, 14]. The physical dimensions of the HP are considered as 890 mm in length (600 mm evaporator length, 200 mm condenser length and 900 mm adiabatic length) and OD= 19.1 mm. Figures 2 and 3 show a comparison of the current model with the literature data for the axial temperature distributions and pressure drop of the HP, respectively. As can be seen, an excellent match has been found with all the data reported.

Table 1. boundary condition for heat pipe analysis

$r=r_o$	$r=r_i$	$r=r_v$	r=0	z=0, L
$q_e''=q_c''=-k_{wall}\frac{\partial\theta}{\partial r}$	$\frac{\partial\theta}{\partial r}=h\theta\ (h=\frac{k_{wick}}{k_{wall}r_i\log(r_i/r_v)});$ $v_l=0$	$v_l=\frac{q''\|_{r_i}}{\rho_l h_{fg}}(\frac{r_i}{r_v})\ \ q''\|_{r_i}=-k_{wall}\frac{\partial\theta}{\partial r});$ $u_v=0$	$\frac{\partial u_v}{\partial r}=0$	$\frac{\partial\theta}{\partial z}=0;$ $u_v=0$

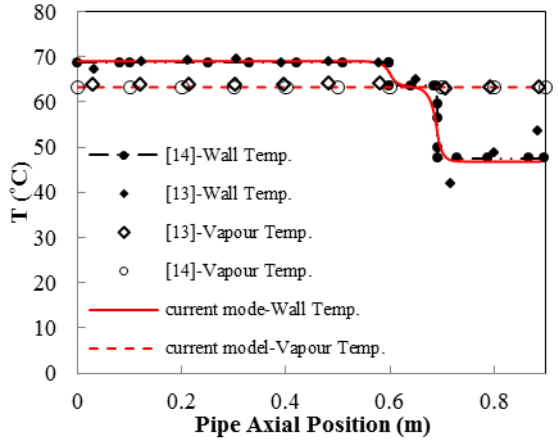

Figure 2. Comparison of the axial distribution of the wall and vapour temperatures.

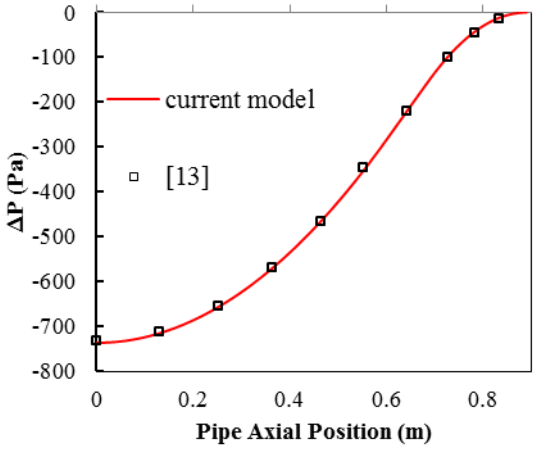

Figure 3. Comparison of the axial liquid pressure drop.

2.1. HP limits

HPs working are strongly dependent on their operational limitations. The operating limitations can be divided into two main categories [23]: the first ones linked to the liquid flow (entrainment, capillary, boiling) and the other ones linked to the vapour flow (viscous and sonic). The most important design consideration is the amount of power that the HP is capable of transferring at a given operational temperature and size (i.e.; length and external radius). The viscous, entrainment and sonic limits are generally much greater in comparison with the capillary limit and so do not pose any constraint [24].

In fact, for the selected temperature range (60-160˚C), the high vapour pressure result in both a small vapour velocity and pressure drop. Therefore, the viscous, sonic, and entrainment limits are typically not reached, allowing the vapour to flow to the condenser section. In the present configuration, only the capillary and boiling limits are affecting the HP performance.
The capillary limit consist in the fact that, for a HP to operate properly, the net pressure drop must be greater than the capillary pressure which is derived from the Laplace-Young equation ($\Delta P_c = 2\sigma_l / r_c$) where σ_l is liquid surface tension and r_c (=$1/2N$) is effective capillary radius of the evaporator wick where N is the screen mesh number.
The other major limitation for the HP is the boiling limit. At higher applied heat flux, nucleate boiling may appear in the wick structure. At steady state operations, an expression for the heat flux beyond which bubble growth will occur may be developed by [25]:

$$Q_b = \frac{2\pi l_{eff} k_{eff} T_v}{\rho_v h_{fg} \ln\left(r_i / r_v\right)} \left(\frac{2\sigma_l}{r_n} - \Delta P_c \right) \tag{12}$$

where l_{eff} is the effective length and r_n is the critical nucleation site radius, which according to [22] ranges from 0.1 to 25.0 μm for conventional metallic case materials.

3. Results and discussion

There are several important factors affecting HP performance: the working fluid, the wick structure, materials, the dimensions and input parameters. In this study the effects of wick thickness, effective pore radius of wick, diameter, evaporator length, power input and heat transfer coefficient of the cooling fluid are analysed to achieve limitations of HP. The effects of these parameters are studied for a copper wrapped screen wick (150 mesh). All the arrangements were investigated at different heat fluxes from 500 to 20000 W/m^2, heat transfer coefficient of 200-1800 W/m^2K and cooling water temperature of 60-160 ˚C. Table 2 shows further values of the design parameters chosen to perform the present analysis, as well as the combinations of these parameters that were analysed. The design parameters shown in the table 3 are fixed for all investigations.

Table 2. Levels of the chosen parameters.

Level	*1*	*2*	*3*	4
l_e [m]	2	1.55	1	0.5
OD [mm]	12.7	20	30	-
t_{wick} [mm]	1	0.75	0.5	0.25
r_c [m]	2.4×10^{-4}	7.9×10^{-5}	3.2×10^{-5}	-

Table 3. Fix parameters.

Wick thermal conductivity [W/mK]	1.97
Wick permeability [m^2]	1.5×10^{-5}
Wall thickness [mm]	0.5
Condenser length [m]	0.17
Adiabatic length [m]	0.04

3.1. Effect of the wick thickness, outside diameter and evaporator length

The selection of the wick for a HP depends on many factors, several of which are closely linked to the properties of the working fluid, the maximum capillary length and the wick permeability. Another feature of the wick that must be optimized is its thickness.
The relationship between wick thickness and vapour temperature are presented in figure 4a, and the effects on the pressure drop for different evaporator lengths and diameters are shown in figures 4b, 4c, and 4d, respectively. As shown in figure 4a, when the wick thickness decreases from 1 mm to 0.25 mm, the vapour temperature decreases because of decreasing thermal resistance of the wick region. It also shows that the vapour temperature is weakly affected by evaporator length, as shown only in the case of OD = 12.7mm. Conversely, the pipe diameter affects the results: the vapour temperature for

OD=30 mm is about 15˚C lower than the temperature for OD=12.7 mm, and its variation with increasing wick thickness is more sensible for the lower outside diameters.

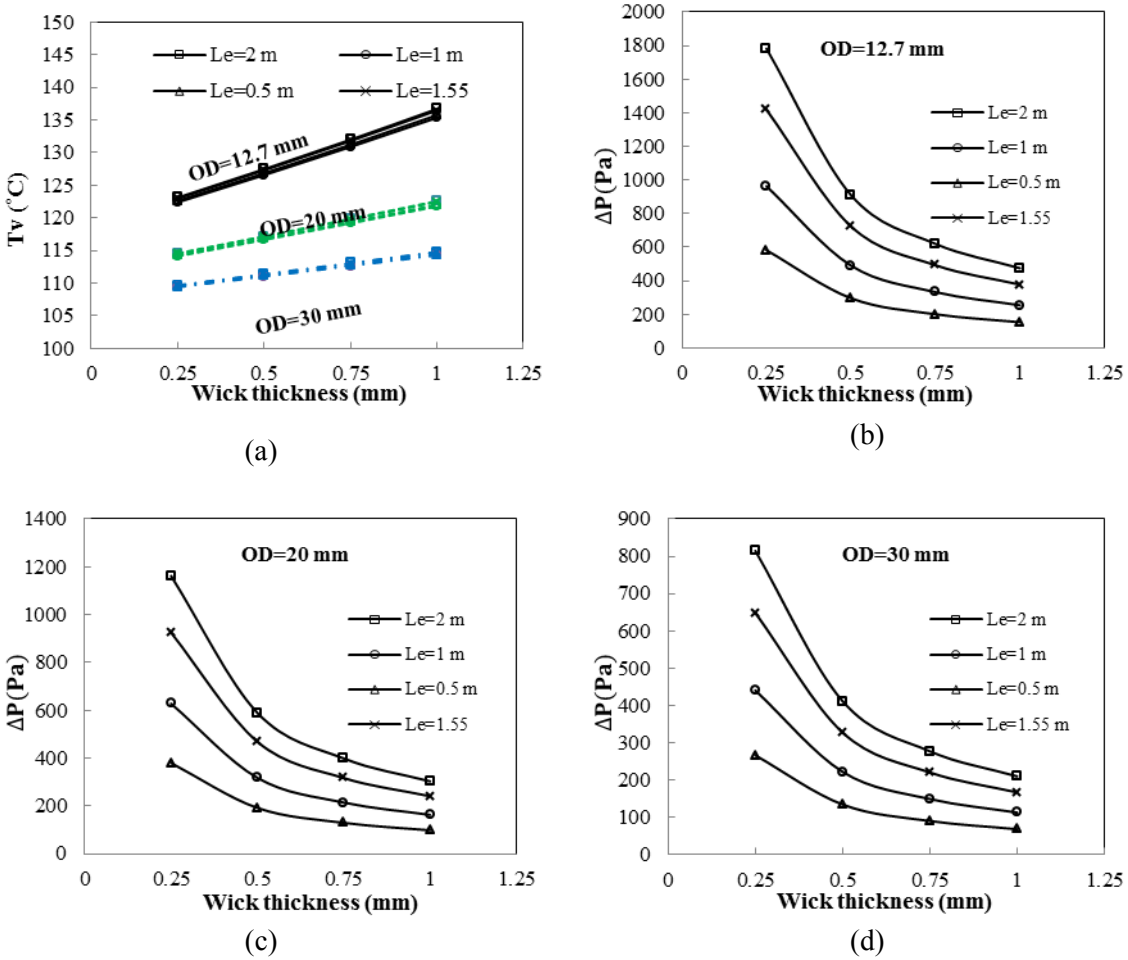

Figure 4. Effect of wick thickness on (a) the vapour temperature (T_v), (b), (c) and (d) the Pressure drop for OD=12.7 mm, OD=20 mm and OD=30 mm respectively for different evaporator lengths.

As indicated in figures 4b-d, the increase in the wick thickness reduces the liquid flow resistance and the pressure drop of liquid decrease too. In addition, when the evaporator length decreases from 2 m to 0.5 m, the slope of pressure drop vs. increasing wick thickness is reduced. It can be found that the evaporator length does not have a significant effect on the vapour temperature, but it does have a significant effect on the pressure drop.

Figure 4d shows also that the decrease of wick thickness, from 1 to 0.25 mm, increases the pressure drop up to 73% for different ODs. From figure 4a it can be seen that the same decrease of the wick thickness reduces the vapour temperature by approximately 10%, 6.5%, and 4% for the HP with OD of 12.7, 20 and 30 mm, respectively.

Figures 4b-d show that when the OD increases, the pressure drop decreases. These results indicate that, when using the HP for medium temperature, it is better to decrease the wick thickness to obtain a lower temperature and HP size. At the same time, we must pay attention to the pressure difference to prevent overcoming the capillary pressure, especially for higher power input.

3.2. Effect of the Heat Transfer Coefficient of the Cooling Fluid

The effects of the variation of heat transfer coefficient of the cooling fluid on the vapour temperature and pressure drop are shown in figures 5a and 5b, respectively. As can be seen, when the heat transfer coefficient increases, the vapour temperature decreases and the pressure drop increases. The influence

of the heat transfer coefficient on the HP performance is less sensible for the higher values of it (after 800W/m^2 K). An increase in the heat transfer coefficient increases the non-uniform distribution of the

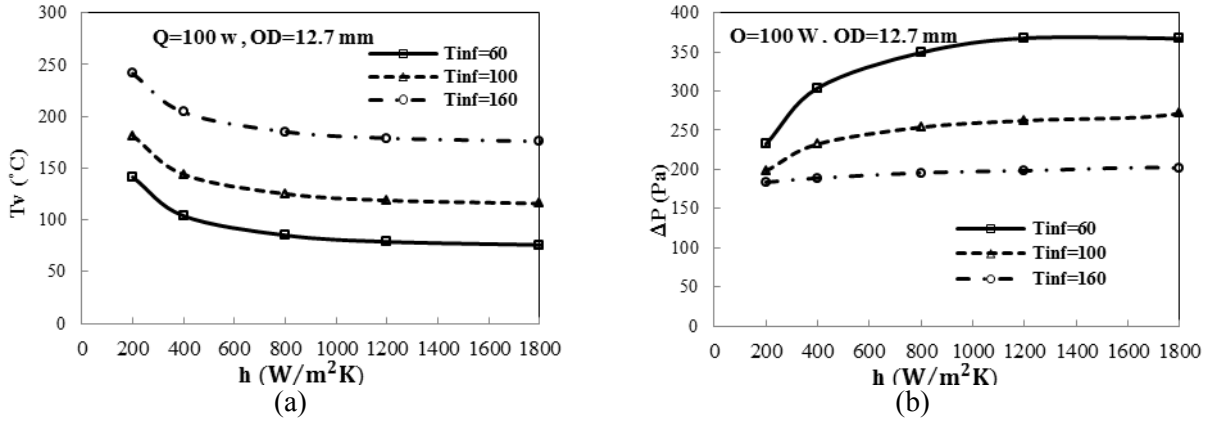

Figure 5. Effect of heat transfer coefficient (h) on a) vapour temperature and b) Pressure drop for different water cooling temperatures ($T_{\inf}$).

heat flux at the wick-vapour interface, and hence, the maximum pressure difference of wick increases and leads to an increase of the total pressure difference. Further, figure 5b shows that increasing heat transfer coefficients does not have a great effect on the pressure drop for cooling water temperature of 160˚C, compared with its effects for lower water temperatures.

3.3. Maximum heat transfer capability (HTC)

For the cooling heat transfer coefficient of 1600 W/m^2 K, the relationship between the maximum HTC and wick thickness is presented in figure 6 for two values of the cooling water temperatures (100˚C and 160˚C), different outside diameters (12.7, 20 and 30 mm), different evaporator lengths (2, 1.55, 1 and 0.5 m), and different effective pore radii (2.4×10^{-4} m, 7.9×10^{-5} m and 3.2×10^{-5} m).

As discussed previously, achieving thin wick is limited by the liquid pressure drop and superheat for the onset of bubble nucleation. As shown in figure 6, in some cases maximum HTC increases with reducing wick thickness and in some cases decreases. This depends on the fact that the boiling limit is less than the capillary limit, or vice-versa.

For instance, in the case of OD=12.7 mm, evaporator length of 2 m and cooling water temperature of 100˚C, as shown in figure 6a, the capillary limit is less than the boiling limit for the wick effective pore radius 2.4×10^{-4} m, therefore HTC decrease with decrease in wick thickness. If effective pore radius changed to 7.9×10^{-5} m, for the wick thickness of 1 and 0.75 mm boiling limit is reached before capillary limit, so HTC increases with a reduction in wick thickness, and the contrary holds for wick thickness of 0.5 and 0.25 mm, because the capillary limit is reached first. A further reduction of effective pore radius leads to improve HTC in the cases that are limited by the capillary pumping.

By increasing OD, when the vapour radius increases, the vapour flow resistance decreases, but the conductive thermal resistance increases, and the size of the HP increases. The effect of the vapour core radius on the HTC is shown in figure 6. As can be seen, when the vapour radius decreases, the maximum HTC does not incur in a significant change, even though the conduction resistance decreases. For example for water cooling temperature of 100˚C, evaporator length of 1 m, wick thickness of 0.5 and effective pore radius of 7.9×10^{-5} m, maximum HTC for OD=12.7, 20 and 30 mm is about 8000 W/m^2. Thus, the overall conductive resistance in the vapour region does not have a considerable effect on the HTC and the heat is transferred mainly by phase change phenomena.

In the analysed range of parameters, the capillary limit was higher than the boiling limit for the wick thickness of 1 and 0.75 mm and for high water temperature (160˚C), but in some cases, for wick thickness of 0.5 and 0.25 mm, the capillary limit was reached before boiling limit (OD=12, 20 mm and $L_e=2$, 1.55 and 1 m). Also, for evaporator length of 0.5 m, in all cases capillary limit was not reached

before boiling limit. Maximum HTC for the water cooling temperature of 100 and 160 ˚C are about 12000 and 5000W/m^2, respectively for the selected configuration as shown in figure 6.

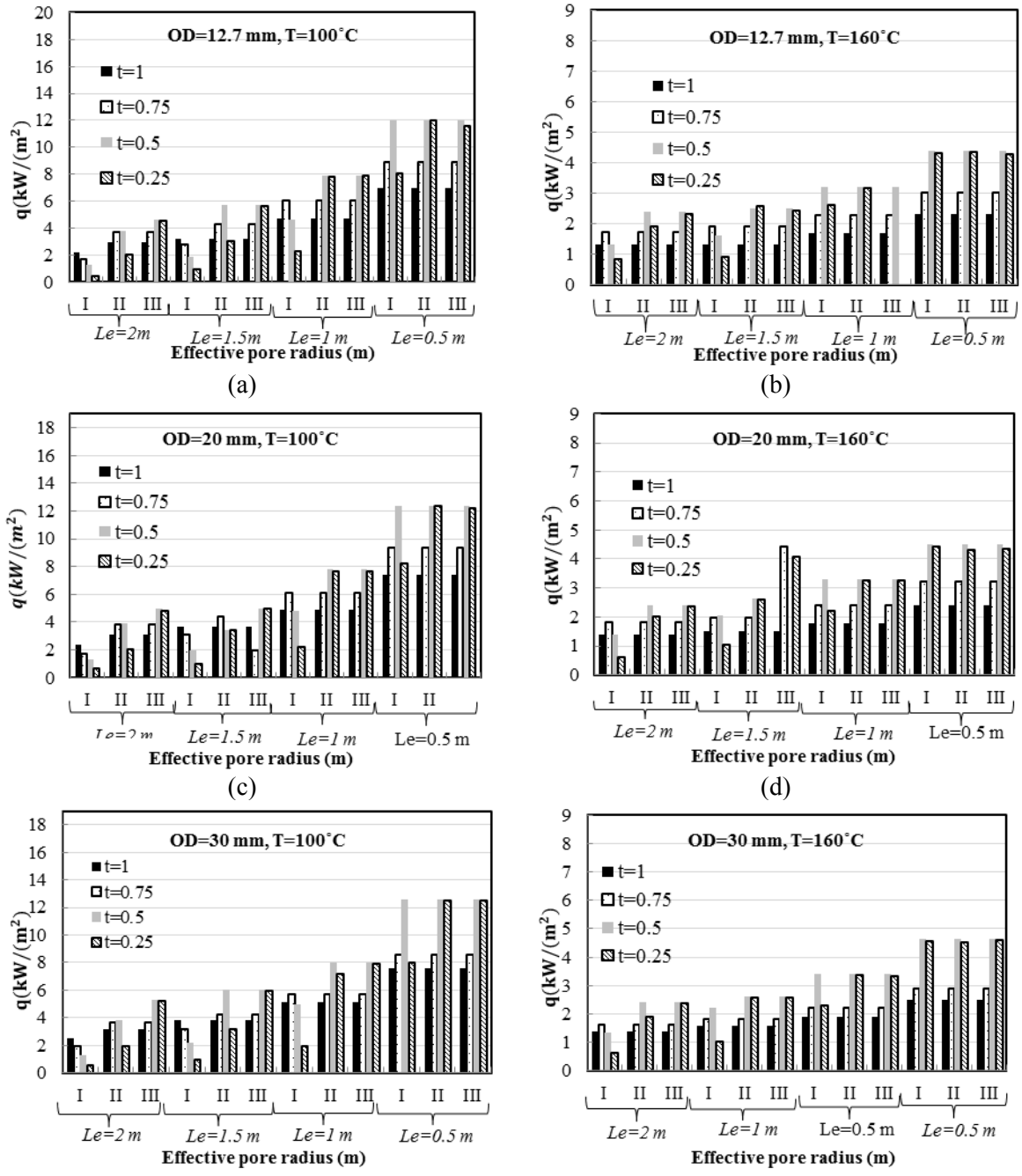

Figure 6. Maximum heat transfer capability for a) OD=12.7 mm, $T_{\inf}=100^{\circ}C$, b) OD=12.7 mm, $T_{\inf}=160^{\circ}C$, c) OD=20 mm, $T_{\inf}=100^{\circ}C$, d) OD=20mm, $T_{\inf}=160^{\circ}C$, e) OD=30 mm, $T_{\inf}=100^{\circ}C$, f) OD=30 mm, $T_{\inf}=160^{\circ}C$ [evaporator length, m (L_e); wick thickness, mm (t); effective pore radius, I=2.4×10^{-4}m, II=7.9×10^{-5}m and III=3.2×10^{-5}m].

Results presented here can effectively direct the design of high heat flux solar device, avoiding capillary and boiling limits, by selecting an appropriate configuration. Results indicate that the optimum wick thickness to achieve maximum heat flux depends on the effective pore radius and

evaporator length. Based on the results of Figure 6, it is concluded that, to reach high input power without limitation, it is advisable to decrease the wick thickness, as it is consistent with the results of Kempers et al. [26], and decreases the pore radius to the smallest possible value. For small wick thicknesses the capillary limit becomes dominant, and the results predict that shorter evaporator lengths yield larger heat fluxes.

4. Conclusions

The heat conduction resistance, the boiling limit and capillary pumping pressure become primary factors determining the maximum HTC in the HP. This paper provides a sensitivity analysis of the issues encountered in the design of HP with specific interest for medium temperature application, typically for solar cooling and industrial process heat. A two dimensional model in the wall coupling the hydrodynamic and thermal models was used in this parametric study to predict the overall HTC. A validation of the numerical model was performed. The results show good agreement between the model results and those found in the literature.

The effects of heat transfer coefficient, power input, evaporator length, pipe diameter, wick thickness and effective pore radius on the vapour temperature, maximum pressure drop and maximum HTC are studied. The results show that the evaporator length has no a significant effect on the vapour temperature in HP for different power inputs. The effect of the heat transfer coefficient on HP performance decreases with increasing its value. The results also show that when the wick thickness increases, the vapour temperature increases, and the maximum pressure difference decreases.

The analysis shows that wick thickness plays an important role in the enhancement of HTC. There is an optimum wick thickness that minimizes the increment of temperatures which independent from the heating power. Results show that it is possible to improve HTC by selecting the appropriate wick thickness, effective pore radius and pipe diameter and evaporator length. By decreasing the wick thickness (until an optimum is reached), because of the decrease thermal resistance of the wick region, HTC can be enhanced. Results also indicate that the maximum dry-out heat flux significantly depends on the wick thickness.

Therefore, an optimal region of HP's lengths and wick characteristic must be chosen to enhance the heat transfer and the heat removal capability especially when the heat fluxes increase. Results of this investigation will assist in optimizing the heat transfer performance of HPs which may contribute to improved HP solar collector design.

References

[1] Rittidech S and Wannapakne S 2007 *Experimental study of the performance of a solar collector by closed-end oscillating heat pipe (CEOHP)* Appl. Therm. Eng. **27** 1978-1985

[2] Franco A and Filippeschi S 2013 *Experimental analysis of Closed Loop Two Phase Thermosyphon (CLTPT) for energy systems* Exp. Thermal Fluid Sci. **51** 302–311

[3] Filippeschi S 2006 On *periodic two-phase thermosyphons operating against gravity* Int. J. Thermal Sci. **45** 124–137

[4] Chun W, Kang YH, Kwak HY and Lee YS 1999 *An experimental study of the utilization of heat pipes for solar water heaters* Appl. Therm. Eng. **19(8)** 807–17

[5] Joudi KA and Witwit AM 2000 *Improvements of gravity assisted wickless heat pipes* Energy Convers. Manage. **41** 2041-2061

[6] Mathioulakis E and Belessiotis V 2002 *A new heat-pipe type solar domestic hot water system* Solar Energy **72** 13–20

[7] Riffat S, Zhao X and Doherty PS 2005 *Developing a theoretical model to investigate thermal performance of a thin membrane heat-pipe solar collector* Appl. Therm. Eng. **25** 899–915

[8] Azad E 2008 *Theoretical and experimental investigation of heat pipe solar collector* Exp. Thermal Fluid Sci. **32** 1666-1672

[9] Brahim T, Foued M and Abdelmajid J 2013 *Parametric Study of a Flat Plate Wick Assisted Heat Pipe Solar Collector* ASME J. Solar Energy Eng. **135** 031016-1

[10] Aghbalou F, Mimet A, Badia F, Illa J, El Bouardi A and Bougard j 2004 *Heat and mass transfer during adsorption of ammonia in a cylindrical adsorbent bed: thermal performance study of a combined parabolic solar collector, water heat pipe and adsorber generator assembly* Appl. Therm. Eng. **24** 2537–2555
[11] Zuo ZJ and Faghri A 1997 *A Network Thermodynamic Analysis of the Heat Pipe* Int. J. Heat Mass Transfer **41(11)** 1473–1484
[12] Xuan Y, Hong Y and Qiang L 2004 *Investigation of Transient Behaviours of Flat Heat Pipes* Exp. Thermal Fluid Sci. **28** 249-255
[13] Tournier JM and El-Genk MS 1994 *A heat pipe transient analysis model* Int. J. Heat Mass Transfer **37** 753-762
[14] Zhu N and Vafai K 1999 *Analysis of cylindrical heat pipes incorporating the effects of liquid e vapour coupling and non-Darcian transport-a closed form solution* Int. J. Heat Mass Transfer **42** 3405-3418
[15] Kaya T and Goldak J 2007 *Three-dimensional numerical analysis of heat and mass transfer in heat pipe* Heat Mass Transfer **43** 775–785
[16] Shabgard H and Faghri A 2011 *Performance characteristics of cylindrical heat pipes with multiple heat sources* Appl. Therm. Eng. **31** 3410–3418
[17] Brahim T and Jemni A 2014 *Effect of the Heat Pipe Adiabatic Region* ASME J. Heat Transfer **136** 042901-1
[18] Vafai K and Wang W 1992 *Analysis of flow and heat transfer characteristics of an asymmetrical flat plate heat pipe* Int. J. Heat Mass Transfer **35** 2087-2099
[19] Vafai K, Zhu N and Wang W 1995 *Analysis of assymetrical disk-shaped and flat plate heat pipes* ASME J. Heat Transfer **117** 209-218
[20] Aghvami M and Faghri A 2011 *Analysis of flat heat pipes with various heating and cooling configurations* Appl. Therm. Eng. **31** 2645-2655
[21] Zhu N and Vafai K 1996 *The effects of liquid e vapour coupling and non-Darcian transport on asymmetrical disk-shaped heat pipes* Int. J. Heat Mass Transfer **39** 2095-2113
[22] Reay DA and Kew PA 2006 *Heat Pipes, Theory Design and Applications* (New York: Elsevier)
[23] Bertossi R, Romestant C, Ayel V and Bertin V 2012 *A theoretical study and review on the operational limitations due to vapour flow in heat pipes* Front. Heat Pipes **3** 023001
[24] Faghri A 1995 *Heat Pipe Science and Technology* (Washington, DC: Taylor and Francis)
[25] Peterson GP 1994 *Heat Pipes: Modelling, Testing and Applications* (USA: John Willey & Sons)
[26] Kempers R, Ewing D and Ching CY 2006 *Effect of number of mesh layers and fluid loading on the performance of screen mesh wicked heat pipes* Appl. Therm. Eng. **26** 589–595